Egyptian Journal of Chemistry

http://ejchem.journals.ekb.eg/

Desulfurization of a Model Liquid Fuel by Adsorption over Zinc oxide/Activated Alumina Assisted with Ultrasonication

Sahar Mohammed Abd Zaid [a], Adnan A. AbdulRazak [a]* and Mohammad Fadhil Abid [b]

[a] *Department of Chemical Engineering-University of Technology, Baghdad, Iraq.*

[b] *Department of Oil & Gas Refining Engineering, Al Turath University College, Baghdad, Iraq.*

Abstract

This study aims to obtain a jet fuel with a sulfur content of less than 15 ppm commensurate with the International Civil Aviation Organization (ICAO) requirements by the sulfur removal of model jet fuels with ultrasound-assisted adsorption for batch systems. A model jet fuel was desulfurized using a modified adsorbent in the present work. The wet impregnation process of Zinc synthesized the adsorbent over activated alumina assisted with ultrasonication in different loading weight percentages of 8.6, 12.2, 18.8, and 22.2wt. %. Experimental results revealed that the best adsorbent performance ratio for Zinc was 18.8wt. %. SEM, EDS, FTIR, XRD, and BET have been used to characterize the prepared adsorbents and evaluate the adsorption process activity. Response surface methodology (RSM), combined with the central composite design (CCD), was used for statistical modeling targeted directly at optimizing the removal process. The critical parameters of initial sulfur concentration, the adsorbent dose, stirring time, and sonication time were investigated for their effect on the process efficiency. The results showed that maximum removal of 68.8 % was obtained at 40 mg/L initial sulfur concentration, 12.3 g/L adsorbent dose, 117 minutes stirring time, and 39 minutes sonication time. The equilibrium data of sulfur adsorption onto ZnO/Al_2O_3 were studied using the linear form of the Freundlich, Langmuir, and Temkin models. Langmuir gives a better fit with a correlation coefficient of R^2 = 0.9985. The resulting kinetic statistics indicated that a pseudo-first-order model for adsorbent represents the adsorption kinetics more accurately with a correlation coefficient of R^2 = 0.9602. Finally, the estimated thermodynamic parameters reveal that the adsorption is endothermic. In addition, the ΔG value, which was inversely proportional with increasing temperature, denotes spontaneity and process feasibility.

Keywords: Adsorptive desulfurization; model; jet fuel; ultrasonication; activated alumina; response surface methodology.

1. Introduction

In recent years, desulfurization research has become imperative due to increasing sulfur content in fuels, stricter environmental regulations, and persistent demands to address challenges by introducing modern materials, material improvements, and developing innovative techniques. Desulfurization of oil products, in general, and jet fuels, in specific, is a complex but necessary process, certainly in emissions, also due to the massive air traffic worldwide[1]. Because of growing environmental concerns, removing organosulfur compounds in jet fuels has gotten much attention[2]. Sulfur oxides, particularly SO_2 (dominant oxide), are discharged into the environment when S-containing fuels are burned, and they may have harmful impacts on human health and the ecosystem. Furthermore, substances might cause the catalyst to deactivate throughout the desulfurization of fuel oil in refineries[3]. Figure 1 depicts the global consumption of jet fuel during (Jan-July 2020), which reveals the immense emissions of sulfur oxides to the atmosphere[4]. The reduction in jet fuel consumption, as observed in Figure 1, was practically due to COVID-19 ban regulations.

*Corresponding author e-mail: adnan.a.alsalim@uotechnology.edu.iq.; (Adnan A. AbdulRazak).
Receive Date: 21 February 2022, , **Revise Date:** 13 March 2022, **Accept Date:** 26 March 2022
First Publish Date: 14 November 2022
DOI: 10.21608/EJCHEM.2022.123060.5504

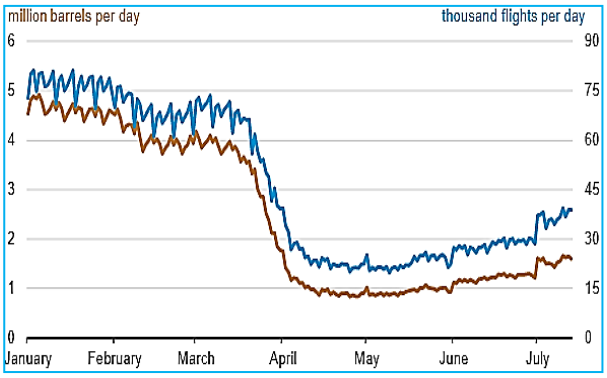

Figure 1. Global jet fuel consumption (Jan-July 2020).[4]

The conventional desulfurization technology implemented by petroleum refineries is the catalytic hydrodesulfurization process (HDS). This technique can efficiently remove the non-refractory sulfur compounds, including Thiols, sulfides, and disulfides. While negligible removal of the so-called refractory sulfur, including Thiophene and its derivatives. This process (HDS) experiences severe difficulties producing ultralow sulfur jet fuel to meet the global requirements (10 ppm). Therefore, a second method was used to complement the HDS process to reach a sulfur content ≤ 10 ppm, in line with international regulations to preserve the environment[5]. Adsorption desulfurization has attracted researchers' interest because of its numerous benefits, including low energy consumption, the capacity to remove refractory sulfur, and the ability to operate at ambient temperature and pressure without the need for oxygen or hydrogen[6]. In the present work, sonication technology was used accompanying the adsorption process. The effect of sonication is expected to change adsorption behaviour by dissociating large molecules into smaller pieces or by changing the surface/opening pores to improve adsorption. As a proof of concept for exploiting the molecular level changes produced by cavitation. Ultrasound has been reported to improve mixing and absorption through cavitation and streaming. In addition, improved absorption has been mentioned as a result of changes in a pore, increased pore size and surface area due to acoustic cavitation [1].

The idea of developing sorbents for selective adsorption of organosulfur elements from liquid fuel has lately gained a lot of traction. Adsorbents with high extraction ability, specificity, and large pore widths to accept sulfur impurities are required for efficient adsorptive desulfurization[7]. The sorbents in this study were prepared using a wet impregnation process and improved by another engineering change was the use of ultrasound to intensify the impregnation process. Ultrasonic technology based on the phenomena of "cavitation" is presented to enhance the impregnation process, consisting of three phases involving the creation, growth, and collapse of bubbles in a liquid. With the collapse of bubbles, an unstable high temperature and high pressure are generated, resulting in an effective and suitable method for mixing solutions, eroding solid surfaces, and facilitating interparticle collisions, which is the reasonable explanation for the formation of smaller particle sizes under ultrasonic radiation. Furthermore, higher metallic dispersion in the synthesis of materials under ultrasonic radiation leads to more active sites and improved catalytic activity without destroying material characteristics. Due to the extreme quicker mass transfer rate, the preparation time may be considerably reduced.

The modification philosophy is that some metals are more favourable on the activated alumina, which correspondingly affects aggregation and dispersion. Thus, nature of alumina, nature of metal, the structure of the porous matrix, the surface area available for modification, metal-metal interactions in multiple metal modifications, repulsive forces due to similar charges and its impact on subsequent metal modifications, partial displacement of one metal by another based on affinity grading and many such complexities associated with metal modification of alumina have posed serious limitations in a priori prediction of metal modifications and its impact on desulfurization. As a consequence, experimental investigations have become imperative for gaining more insight. It's worth noting that the metallic alteration reduces surface area while increasing the number of acidic oxygen functional groups on the adsorbed surface[1,8,9].

As in adsorptive desulfurization process, the active adsorbent is located on a porous, non-reactive substrate that enables high surface area for the adsorption of sulfur compounds. Adsorption occurs S-molecules attach to the sorbents and remain there separate from the fuel. Various researchers have employed this approach for the removal of sulfur from numerous forms of fuels and model oils by varying adsorbent materials [10].

Alumina has good adsorptive properties, so it's utilised to remove organic compounds from aqueous solutions [11] as well as surfactants such as sodium dodecyl and octylphenol from single and multi-surfactant aqueous

solutions [12]. Different researchers have utilized it for the adsorptive removal of phosphate [13]; Co (II), Ni (II), Cu (II), and Cr (II) [14]; Zn(II) [15]; and dibenzothiophene (DBT) sulfone, etc [16]. In a recent study, Etemadi and Yen [16] The discrepancy in the adsorption capacity of amorphous acidic alumina and crystalline boehmite for the adsorption of dibenzothiophene (DBT) sulfone in the ultrasound-assisted oxidative desulfurization process was explained using several characterisation approaches. Kimet al. [17] in a fixed-bed adsorption system, researchers investigated adsorptive desulfurization using a model fuel and three common adsorbents (activated carbon, activated alumina, and nickel-based adsorbent). However, little attempt was made to investigate the technical components of the adsorption process, such as kinetics, isotherms, and thermodynamics. Furthermore, relatively few adsorptive desulfurization studies have focused on these critical engineering features of adsorption system design.

In the pioneer Iraqi petroleum refinery (i.e., Dora refinery), sulfur is removed from petroleum distillates using the HDS method to produce jet fuel of about 50 parts per million sulfur content[18]. This study aims to obtain a jet fuel with a less than 15 ppm sulfur content commensurate with ICAO "International Civil Aviation Organization" requirements. Moreover, the improved jet fuel will enhance global environmental protection and reduce the negative impacts on human health and the environment[19]. The present work included synthesizing adsorbents material (ZnO/Al_2O_3) by the wet impregnation process with ultrasonication using activated alumina as support by single metal impregnation for zinc in different loading weight percentages. In addition, the impact of key operational factors on the effectiveness of desulfurization treatment operations in a batch system was explored. There were additional talks about the kinetics, thermodynamics, and isotherm models of the desulfurization process.

2. Materials and Methods

2.1. Materials

Zinc nitrate [chemical formula "$Zn(NO_3)_2.6H_2O$", 297.49 g/mol, 99.9% purity] and Thiophene (C_4H_4S) [99% purity, 84.16 g/mol, 84°C boiling point] were supplied from Sigma-Aldrich. Cyclohexane (C_6H_{12}) [81.162 g/mol, 83.74C° boiling point, 99.5% purity] was obtained from SDFCL, S D Fine-Chem Limited, India. Activated alumina (Al_2O_3) pellets (3mm average size) were received from the "Petroleum Research and Development Center/ Iraqi Ministry of Oil". The Pellets were crushed, grounded, and sieved by Sieving Analysis to obtain a 125μm screen average size.

2.2. Methods

2.2.1 Synthesis of ZnO/Al_2O_3

The adsorbent was prepared using the wet impregnation technique assisted with ultrasound. Activated alumina was used as a support material and zinc nitrate as a metal precursor to obtaining different weight loadings of 8.6, 12.2, 18.8, and 22.2 wt% as follows: various $Zn(NO_3)_2{\cdot}6H_2O$ salt weights was dissolved in distilled water. Al_2O_3 was added to the zinc-nitrate precursor. Sonicated for 30 min with ultrasonic bath (ultrasonic cleaner set WUC-D06H). The impregnation process occurred under continuous stirring using a magnetic stirrer at room temperature and 300 rpm. The salt was filtered by Buchner funnel with a vacuum pump. It was dried in an oven at 110 C° overnight. The adsorbent was taken to calcination in a programmable electrical furnace at 500 C° for five hours. A block schematic of the adsorbent preparation process is shown in Figure 2.

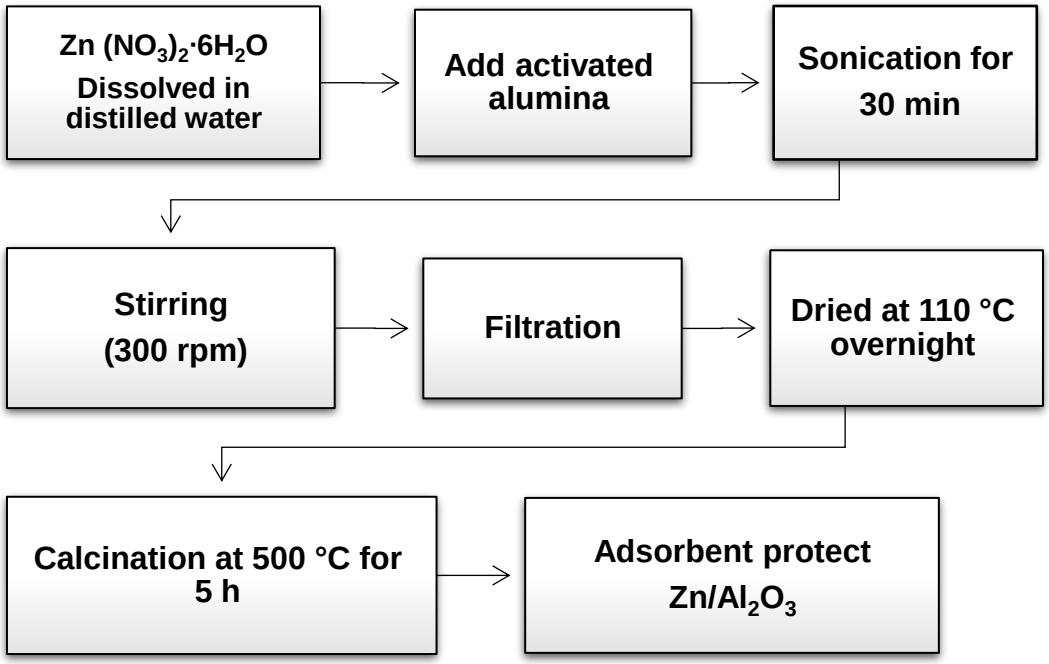

Figure 2. Schematic algorithm of the adsorbent preparation.

2.2.2. Characterization

The ZnO/Al_2O_3 was characterized using SEM, EDX, XRD, BET, and FTIR. A Scanning Electron Microscope [Model: INSPECT S50] was used to conduct SEM and EDX. The XRD measurements were performed with an X-ray diffraction analyzer [Shimadzu-6000, Japan]. The BET technique (Brunauer, Emmett, & Teller) was acted with using a surface area detector [Type: S-surfs 8700, USA]. The FTIR analysis was carried out using Fourier transforms infrared spectroscopy [Model: The Spectrum Two N system, high-performance FT-NIR, Perkin Elmer].

2.2.3 Adsorbent performance test

After preparing the adsorbent material with various metal loading percentages on the surface of activated alumina, batch mode experiments were conducted for sulfur removal using the prepared adsorbents the following conditions: 40 ppm initial sulfur concentration, 10 g/L adsorbent dose, 120 min contact time, 40 min sonication time, and 500rpm stirring speed. The liquid phase was separated from the adsorbent and then reserved for the sulfur analysis device. Then the adsorption capacity of each loading ratio was calculated.

2.2.4 Design of Experiments and Statistical Data analysis

Different chemical and physical processes may benefit from the usages of the response surface technique, a statistical technique [20, 21]. The response surface method (RSM) and central composite design were utilized in this work to assess and design the experimental data for sulfur removal using the application Design-Expert "CCD". The goal of applying this method was to find out how to relate the response (sulfur removal efficiency) to the operational factors that influence the removal process to get maximum removal. Initial sulfur concentration (ppm), adsorbent dosage (g), contact time (min), and sonication time (min) were all investigated in this study at three levels: low, medium, and high. Table 1 provides the encoded limits for these variables.

Table 1. The levels of the different factors were used for experimental runs.

Factors	Notation	Range and levels		
		Low Level	Central Level	High Level
Initial sulfur concentration(ppm)	A	40	60	80
Adsorbent dose (g/L)	B	7.5	10	12.5
Stirring time (min)	C	60	90	120
Sonication time (min)	D	20	30	40

2.2.5 Desulfurization process

Batch system

Batch adsorption tests were performed by adding 7.5, 10, and 12.5 g/L of adsorbent dose to a model fuel prepared of different initial concentrations of 40, 60, and 80 ppm in Cyclohexane. Then, Sonication was conducted for the different periods of 20, 30, 40 min by an ultrasonic bath (60 kHz frequency & 425 Watts power). After that, stirring was curred out at 500 rpm for all experiments. Mixing time was varied at 60, 90, 120 min. The mixture was filtered using filter paper "Whatman No. 42". The filtrate was stored for analysis by the sulfur analysis device (monochromatic wavelength dispersive X-ray fluorescence ASTM D-7039). The elimination effectiveness (percent R) and adsorption capacity (mg/g) were calculated using the following equations[22]:

$$\%Removal = \frac{Ci-Ce}{Ci} \times 100 \quad (1)$$

$$\text{Adsorption capacity } (q_e) = \frac{Ci-Ce}{w} \times V \quad (2)$$

Where C_i and C_e are the initial and final concentrations, respectively (mg/L), V is the volume of adsorbate (L), and W is the adsorbent weight (g).

Adsorption isotherm models

Langmuir isotherm: The creation of monolayer adsorption with equal heat of adsorption on the surface is assumed in this model[23]. The following is a representation of the linearization form[24]:

$$\frac{Ce}{qe} = \frac{1}{qmax} Ce + \frac{1}{qmax\ b} \quad (3)$$

Where q_{max} is the Langmuir constant associated with adsorption capacity (mg/g), b: constant refers to the adsorption energy (L/mg). The slope of the linear plot of C_e/q_e versus C_e may be used to determine the constants q_{max} and b from Eq. (3). Furthermore, the Dimensionless equilibrium parameter R_L indicates whether the isotherm is favorable, unfavorable, irreversible, or linear when $R_L < 1$, $R_L > 1$, $R_L = 0$ and $R_L = 1$, respectively. Eq. (4) expresses it as follows:

$$RL = \frac{1}{1+bCi} \quad (4)$$

Freundlich isotherm: The surface energy is defined by using the equation provided by[25]:

$$ln\ qe = ln\ Kf + \frac{1}{n} lnCe \quad (5)$$

Where K_f is a constant related to the sorbet's adsorption capacity, and n is the adsorption intensity based on n's value poor adsorption, moderate adsorption, and good adsorption are observed when the value of $n < 1$, $n = 1$–2, and $n = 2$–10, respectively[26].

Temkin isotherm: Temkin's isotherm model may be represented in a linearized form as[27]:

$$qe = B\ ln\ Kt + B\ ln\ Ce \quad (6)$$

Where K_t: The maximum binding energy is represented by the equilibrium binding constant (L/g), B = RT/b is the Temkin constant (J/kJ), b: is the adsorption heat (kJ/mole), R: is the universal gas constant (8.314 J/mol. K), and T: is the absolute temperature (K).

Adsorption kinetics

First-order kinetic: The pseudo-first-order kinetic model was used to analyze the kinetic data. The model's linear form is provided in eq (7) [28, 29]:

$$log(qe - qt) = log\ qe - \frac{K1}{2.303} t \quad (7)$$

Where q_e is the amount of sulfur adsorbed at equilibrium (mg/g), q_t is the amount of sulfur adsorbed over time (mg/g), and K_1 is the constant equilibrium rate of the pseudo-first model (1/min). The slope and intercept of the linear plot may be used to calculate the rate constant K_1, the adsorbed quantity at equilibrium (q_e), and the values of R^2.

Second-order kinetic

The pseudo-second-order kinetic interaction is represented in eq (8)[30]:

$$\frac{t}{qt} = \frac{1}{k2\ qe^2} + \frac{t}{qe} \quad (8)$$

Where K_2: is the rate constant for sorption (g/mg.min). (t/q_t) was plotted vs the time to get K_2 and q_e for this kinetic model.

Intra-Particle diffusion

The potential of intra-particle diffusion is symbolized through this model, as shown in the eq. (9)[31]:

$$qt = Kp\ t^{0.5} + I \quad (9)$$

Where K_P: refers to the constant rate (mg/g.min$^{-0.5}$) and I: denotes the constant intra-particle diffusion.

Adsorption Thermodynamics

The thermodynamics analysis focuses on the temperature change because it impacts how much a substance can be adsorbed. Thermodynamic measures such as a change in enthalpy (ΔH°), entropy (ΔS°), and Gibbs free energy (ΔG°) can be used to assess the naturalness and viability of a process. These variables are calculated from the equation of Van't Hoff through using Eqs. (10, 11, and 12) [32]:

$$\Delta G = -RT\ ln\ KL \quad (10)$$

$$KL = \frac{qe}{ce} \quad (11)$$

$$lnKL = \frac{\Delta s^\circ}{R} - \frac{\Delta H^\circ}{RT} \quad (12)$$

Where K_L denotes the distribution coefficient expressed as $K_L=q_e/C_e$, T denotes the absolute temperature (K), and R denotes the gas constant (8.314 J/kmol). From the slope and intercept between lnK_L and 1/T, the values of ΔH° and ΔS° are estimated.

3. Results and Discussion

3.1. Impregnation method

The loading percentages were obtained by controlling the main factors affecting the mineral impregnation process, namely the impregnation time and the amount of metal nitrate added. The required loading percentages were achieved by controlling these variables, as shown in Table 2.

Table 2. Loading percentages for ZnO/Al_2O_3

Adsorbent	Time of impregnation (h)	Amount of Zinc nitrate (g.)	Zn loading (wt. %)
ZnO/Al_2O_3	24	200	8.6
	36	230	12.24
	48	278	18.8
	48	320	22.24

It was observed from Table 2 that increasing the amount of nitrate resulted in a higher loading rate. This higher loading rate was associated to the fact that as the amount of metal nitrate in the solution increases, the number of metal atoms transferring to the active sites of the adsorbent surface increases. Moreover, the immersion time was an essential factor directly related to the loading rate until the saturation level was achieved. More metal may be transported to the alumina with longer interaction duration between the carrier and the metal nitrate precursor. Experimental results are listed in Table 2.

3.2. Adsorbent performance test and effect of metal modification

Table 3 shows the results of the sulfur adsorption test on ZnO/Al_2O_3. As observed in Table 3, the adsorbent with 18.8 wt% showed the highest adsorption capacity. However, the over Loading of metal at 22.2 wt. % causes blockage of the pores of the support activated alumina during sequential impregnation steps. Therefore, the adsorbent of higher metal loading does not offer good performance, evident from the decrease in adsorption capacity. Hence, the metal loading of 18.8% wt. was chosen to conduct sulfur removal process experiments.

Table 3. Adsorption capacity for each loading ratio

Adsorbent	Loading (wt. %)	Adsorption capacity (mg/g)
Al_2O_3	0	3.93
ZnO/Al_2O_3	8.6	4.46
	12.2	5.50
	18.8	6.82
	22.2	6.03

3.2.1 Impact of metal modification on the Desulfurization process

Desulfurization experiment was conducted to evaluate the effect of metal loading with different loading ratios on desulfurization performance, as shown in Table 3. It was found that when compared to Al_2O_3, the modified adsorbents have a relatively excellent Thiophene adsorption capability. The mechanism of metal addition to alumina alteration might be fairly complex. The main objective is to use electrostatic interactions between positively charged metal species to eliminate a slightly polar, negatively charged sulfur moiety [33-35]. According to numerous researchers, the nature of these associations can be attributed to coupled or individual interactions of π–complexation, metal–sulfur bonding, and/or acid–base interaction. Interactions with metals, might enhance adsorption capacity, and as a result, sulfur removal. On the other side, sulfur adsorption capacity and selectivity of the adsorbent could be further improved by modifying different kinds of active surface sites for sulfur adsorption, such as Lewis sites, useful functional groups, and electronic defect centres, micro-structural defects, etc. According to Lewis acid-base theory, most sulfur compounds (Thiophenic) in jet fuels are Lewis-bases, easily adsorbed at Lewis acid sites. As a result, materials with strong Lewis acid sites may be engineered and chosen to selectively adsorb sulfur compounds containing a lone pair in jet fuels. The Lewis acid-base adsorption mechanism involves the interaction of acid sites on the adsorbent's surface with Thiophene [36, 37].

3.3 Characterization of ZnO/Al_2O_3

3.3.1 Scanning electron microscopy (SEM)

Figure 3 shows the structural morphologies of Al_2O_3 and ZnO/Al_2O_3 that were investigated using SEM analysis. The SEM photos depict randomly dispersed particles of various geometries and sizes along agglomerates in the shape of uneven morphology plates of samples. It demonstrates that Zn is evenly distributed throughout the whole surface of the alumina, confirming that the impregnation was successful. The existence of the substrate and metal was confirmed, allowing the components present in the catalytic system to be identified.

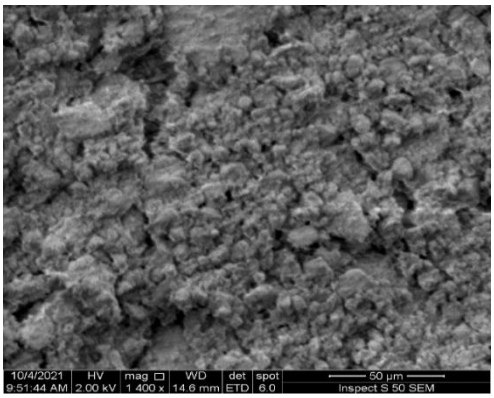

(a)

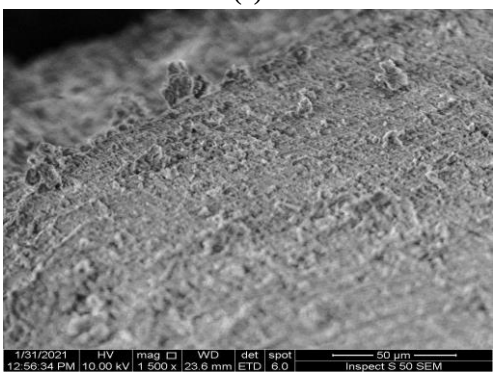

(b)

Figure 3. Typical SEM image for (a) Al_2O_3; and (b) ZnO/Al_2O_3

3.3.2 EDAX "Energy dispersive x-ray analysis"

An Energy Dispersive X-ray Spectrometer was utilized to investigate the mineralogical and chemical composition of the adsorbents employed in the adsorption investigation. According to the proportions given in Figure 4(a-d), the adsorbent contains mostly oxygen, aluminum, and metal loaded (Zn). The presence of Zn metal in the EDX spectrum is around 8.6, 12.2, 18.8, and 22.2 weight percent, respectively.

3.3.3 XRD "X-ray diffraction" analysis

XRD analysis was used to evaluate the phase transition of the Al_2O_3 support. By comparing it with the standard XRD pattern, it was indicated that it was Activated alumina[38]. The lattice spacing of alumina and conventional XRD are compared. Strong peaks at 2θ values of ~ 66.8606, 38.2352, and 43.2318 as in Figure 5a.

The X-ray diffraction patterns of ZnO/Al_2O_3 are shown in Figure 5b. The ZnO/Al_2O_3 adsorbent shows strong peaks at 2θ values of ~37.0861°, 66.6138°, 31.4915° this result could be related to the metal particles' diffusion in the alumina matrix during the calcination step, leading to the zinc alumina spinel phase formation. Compared with activated alumina, the appearance of new strong peaks indicates metal loading on its surface. The more metal is loaded results in higher metal peaks

3.3.4 FTIR "Fourier-transform infrared spectroscopy"

The chemical structure of an adsorbent has an emotional significance in recognizing the process of adsorption. The FTIR technique is a significant tool for identifying the characteristic functional groups on the surface of the samples in Figure 6, which are instrumental in the adsorption of chemical compounds. The spectral range varied from 4000 to 450 cm^{-1} for the activated alumina (Figure 6a) and ZnO/Al_2O_3 (Figure 6b). The FTIR of activated alumina in Figure 6a shows that the peaks are shown at 3376.5 cm^{-1}, 1645 cm^{-1}, and 1096.22 cm^{-1} stretching of the alumina-alumina bond. For understanding alumina-bonding patterns, the ion stretching region is helpful. At wave numbers between 1000 and 3500 cm^{-1}, the intensities reduced. Asymmetrical stretching has been assigned to this peak. Figure 6b shows that the OH stretching vibration is responsible for the broadband at 3447 cm^{-1}, while the CO, C=O, and CO_2 groups are responsible for the other bands at 1371, 1500, and 1630 cm^{-1}. The FTIR spectrum displays an absorption peak at roughly 497 cm^{-1}, which is the Zn–O bond of ZnO's distinctive absorption peak. Al-O stretching vibrations were responsible for the two large absorption bands at about 610 cm^{-1} and 747 cm^{-1}.

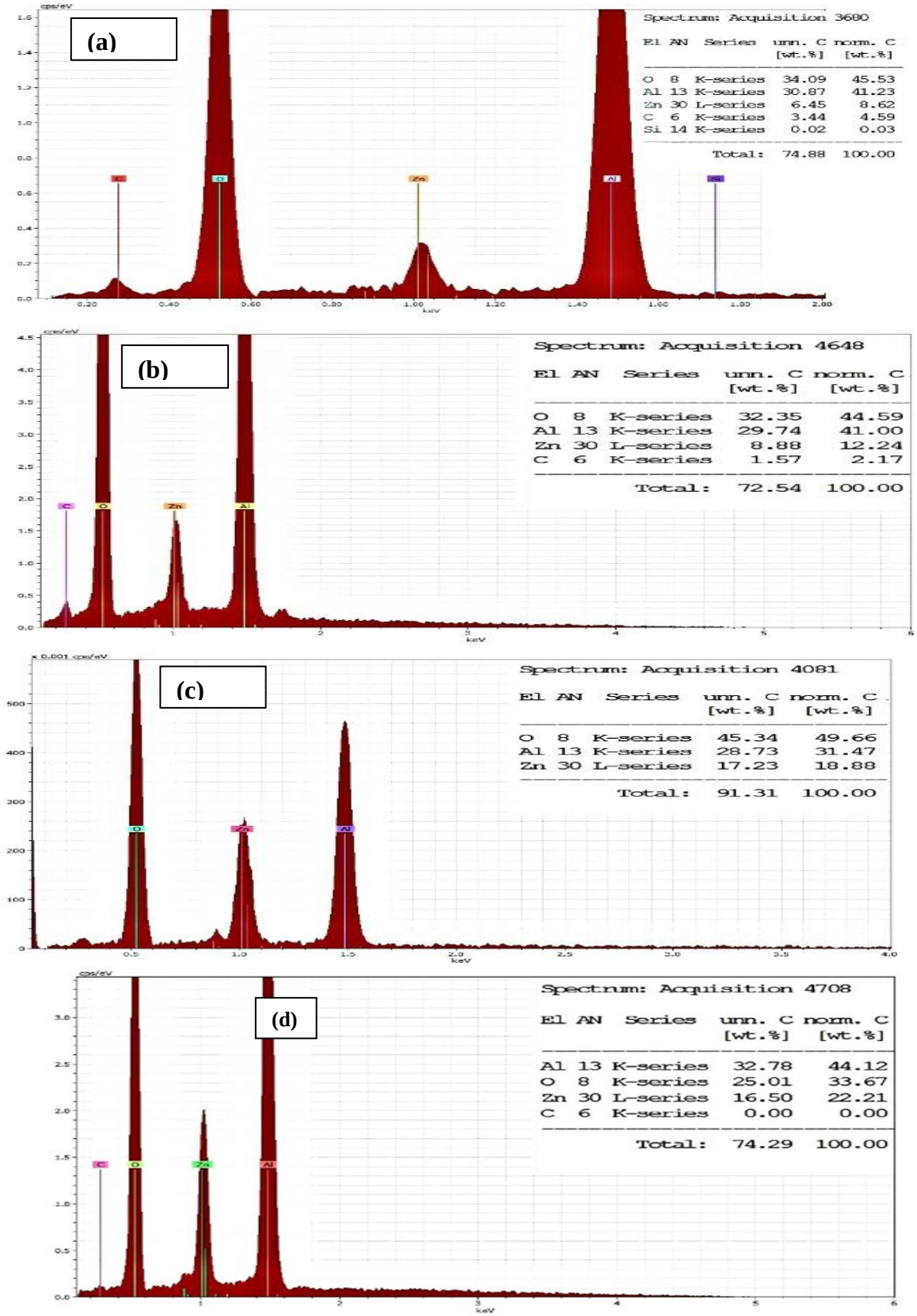

Figure 4. Typical EDAX for the ZnO/Al_2O_3 adsorbent (8.6%, 12.2%, 18.8%, 22.2) respectively

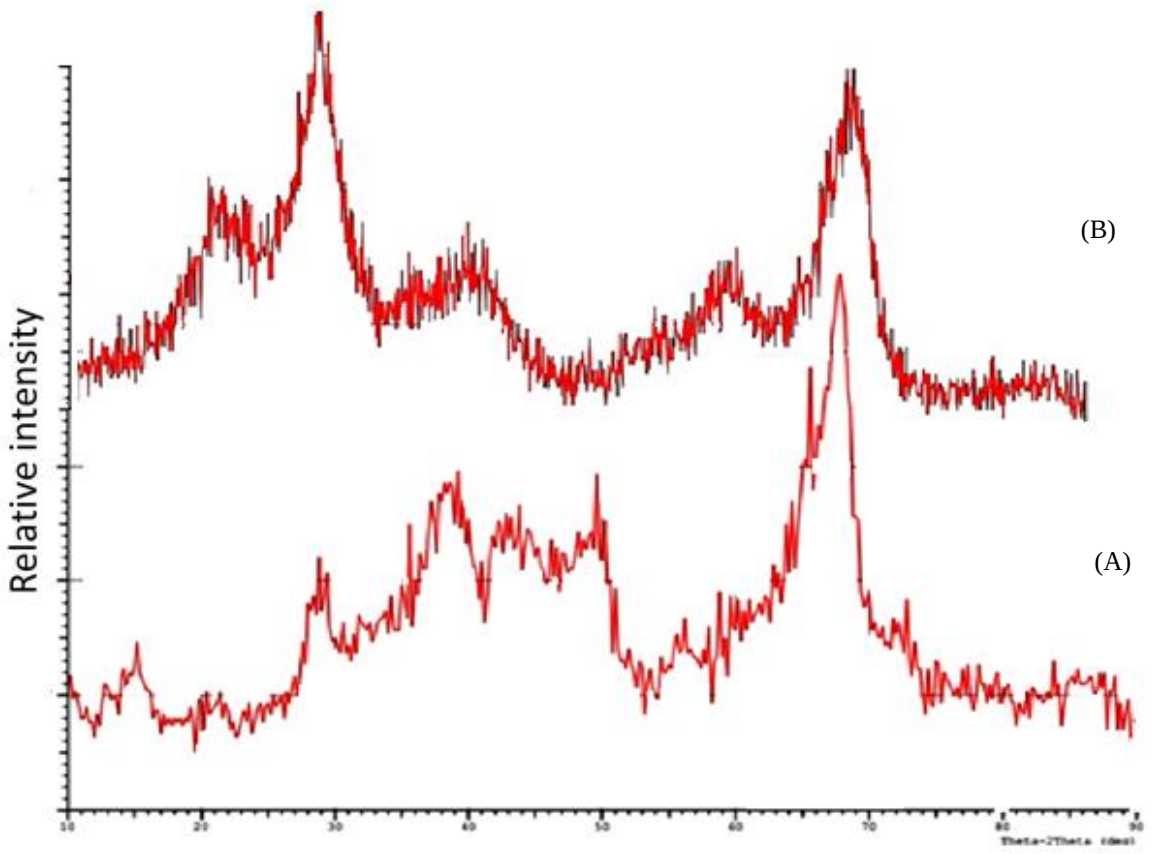

Figure5. XRD Patterns of (a) Al_2O_3, (b) ZnO/Al_2O_3 (18.8 wt %).

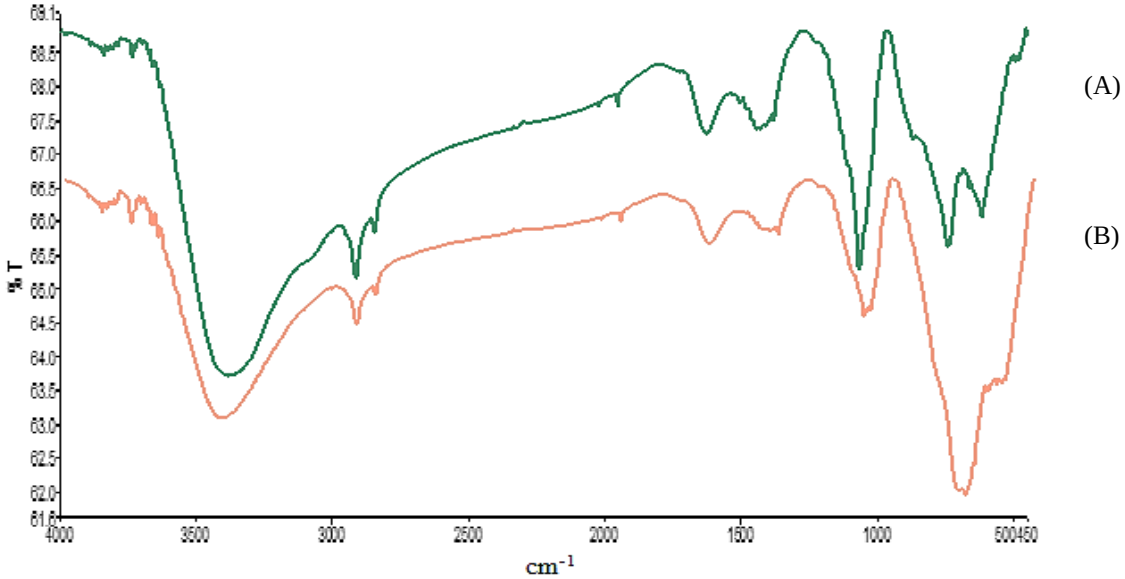

Figure 6. FTIR spectra of (A) Al_2O_3, (B) ZnO/Al_2O_3 (18.8 wt %).

3.3.5 Measurements of surface area (BET)

It is vital to consider the surface area and pore volume of the catalyst support because excessive surface area contributes to high active sites, which causes rising inactivity. Table 4 displays the adsorbent ZnO/textural Al_2O_3's characteristics. The specific surface area for alumina decreases after impregnation with an overall metal content increase because the metal particles occupy a part of this space, which means that the process of impregnation has been successful.

Table 4. The Al_2O_3 and ZnO/Al_2O_3 texture properties.

Adsorbent	Surface area (m^2/g)	Pore volume (cm^3/g)
Activated alumina (Al_2O_3)	285	0.62
ZnO / Al_2O_3 (18.8 wt%).	231	0.51

4. Central Composite Design (CCD) model's results

The CCD method investigated the relationship between sulfur removal efficiency (R %) and process factors. Based on regression analysis technique, the equation below reveals the objective function (i.e., adsorption efficiency) as a function of operating parameters'

$$Removal\% = -134.15485 - 0.429228A + 6.69335B + 2.21015C + 2.53996D - 0.072541AB - 0.005355AC + 0.003135AD - 0.014389BC - 0.000768BD + 0.001014CD + 0.008341A^2 + 0.129844B^2 - 0.008409C^2 - 0.042135D^2$$

Where, R: sulfur removal, A: initial sulfur concentration (ppm), B: adsorbent dose (g/L), C: reaction time (min) and D: sonication time (min).

A positive sign in the preceding equation implies that increasing the variable's value increases sulfur removal. Concurrently, the negative sign depicts that the value of the variable results in a decrease in sulfur removal.

The interaction effect is represented by two variables, whereas the second-order term of the variables represents the square effect. The response surface method (RSM) was used to identify the major factors in the desulfurization process.

5. ANOVA analysis

In the designed experimental technique, an ANOVA test was utilized to determine the relevance of each factor. The ANOVA test is examined from the user's perspective, emphasizing the model's design and the assumptions that underpin the procedure. To visualize the ANOVA model and interpret the data, it is advised to utilize a graphical method. The primary ANOVA models have already been updated with some more extensive material regarding one-factor ANOVA, cross-design, interaction designs, repeated ANOVA measurements and estimate of variance components. The F statistic may be thought of as a ratio of two variances. A measure of dispersion, or the degree to which data depart from the mean, is the variance. F should be greater than the value selected for the F distribution if the model is considered an ideal indicator of the pilot program's effectiveness. Table 5 shows that Model F has an important ZnO/Al_2O_3 ratio of 78.39. When P falls below 0.05, it is common to use the P-value to determine whether or not the F distribution is statistically significant. There is a significant lack of fit, as shown by an F-value.

The R^2 and R (adj.): R^2 indicate whether or not the software is reliable in its outcome prediction. Table 6 shows that R^2 and (adj.) R^2, in this case, suggests an adequate degree of appropriateness (goodness-of-fit).

The coefficient of determination (R^2) was used to estimate the models' fit, shown in Table 6. The R^2 value was high (nearly one), acceptable and reasonable with the empirical data's quadratic model.

6. Operational variables' impact

Two- and three-dimensional contour plots and response surfaces were used to illustrate the theory. 3D response surface shows the dependent variable, sulfur removal, against two independent variables if other factors remain constant. These 2D contour plots, like 3D response surface plots, are useful for studying the influence of independent variables on response. Using two-dimensional contour plots, we can see how the independent variables interact with one another.

Table 5. The ANOVA results of the quadratic model for sulfur removal

Source	Sum of Squares	df	Mean Square	F-value	p-value	
Model	5718.62	14	408.47	78.39	< 0.0001	significant
A-initial concentration	2111.70	1	2111.70	405.27	< 0.0001	
B-dose	1474.01	1	1474.01	282.89	< 0.0001	
C-time	1109.41	1	1109.41	212.92	< 0.0001	
D-sonication time	144.74	1	144.74	27.78	< 0.0001	
AB	210.49	1	210.49	40.40	< 0.0001	
AC	165.17	1	165.17	31.70	< 0.0001	
AD	6.29	1	6.29	1.21	0.2892	
BC	18.63	1	18.63	3.58	0.0781	
BD	0.0059	1	0.0059	0.0011	0.9736	
CD	1.48	1	1.48	0.2841	0.6018	
A^2	28.84	1	28.84	5.54	0.0327	
B^2	1.71	1	1.71	0.3275	0.5756	
C^2	148.41	1	148.41	28.48	< 0.0001	
D^2	46.00	1	46.00	8.83	0.0095	
Residual	**78.16**	**15**	**5.21**			
Lack of Fit	78.11	10	7.81	808.03	< 0.0001	significant
Pure Error	0.0483	5	0.0097			
Cor Total	**5796.78**	**29**				

Table 6. Coefficient of determination (R^2) of the desulfurization process

ZnO/Al_2O_3 (18.8 wt %).	
R^2	0.98
Adjusted R^2	0.97
Predicted R^2	0.91
C.V. %	6.12
Std. Dev.	2.28

6.1. The Influence of Adsorbent Dose and Initial sulfur Concentration

Figure 7A depicts the influence of the initial sulfur concentration on the removal process, which indicates that increasing the initial concentration decreases the sulfur component's removal rate. This trend is because each ZnO loaded-adsorbent has a finite number of active sites on its surface that become saturated at a particular sulfur concentration [39, 40].

The desulfurization of Thiophene was also investigated using different adsorbent doses of (7.5, 10, and 12.5). The influence of adsorbent dose on desulfurization is shown in Figure 7Aa. The increased percentage of sulfur removal with the increased amount of adsorbent dose can be due to the availability of a higher surface area for adsorption. The adsorbent surface becomes saturated with Thiophene when a low adsorbent dose is utilized (i.e., the accessible surface area is less than optimal or necessary). A substantial amount of residual Thiophene is retained in the solution. Because a more accessible adsorbent increases sulfur adsorption, a constant rise in adsorbent dosage, greater surface area, and active sites increase sulfur removal. As shown in Fig. 7Aa, the percentage elimination of Thiophene becomes almost constant when applying an adsorbent dosage greater than necessary. This result agrees with the findings of [41].

6.2. Effect of initial concentration and Time

Figure 7B illustrates the variation of sulfur removal against initial sulfur concentration and operational time. As seen in Figure 7B that during the first 90 minutes of treatment, the sulfur content dropped dramatically. However, the residual sulfur content reduces steadily when the contact period is increased from 100 to 120 minutes. After more than 120 minutes, the equilibrium is almost reached, and this is long enough to provide adequate sulfur elimination. This behavior is attributed to that during the first stage; there are several vacant places on the surface area that could be used for adsorption. Moreover, repulsion forces between the molecules in solid and bulk phases eventually make it impossible to fill all of the remaining vacant spaces.

Furthermore, the sulfur is adsorbed into macro and meso-pores, becoming almost saturated throughout the adsorption process. Following that, molecules must travel farther and deeper into the micro-pores, experiencing far more resistance. As a result, the

adsorption rate slows down as time passes. It was concluded that the increase in contact time has a positive effect on the removal process; the largest number of sulfur atoms travel to the adsorbent until the equilibrium state is reached. Previously published data of [42, 43] confirmed our outcomes.

6.3. Effect of initial concentration and Sonication time

Figure 7C shows the sonication process effect in gradually increasing the efficiency of the removal process, reaching its strongest effect at the 40th minute. It is predicted that the cavitation process could change the adsorption behavior by disintegrating bigger molecules into smaller fragments to accommodate the adsorption process. Cavitation has a physical as well as a chemical influence. The physicochemical changes are primarily caused by the production of extreme temperature (~10,000 K) and pressure (~1000 atm) conditions at the pico-scale as a result of the cavitation process's implosion of cavities, which can then cleave the molecules. This makes it easier for molecules to flow through the pores of the adsorbent substance[37, 40].

6.4. Time and adsorbent dose effects

Figure 7D demonstrate a growing trend in the removal process with increasing duration and adsorbent dosage. It's a well-established fact that as time passes, more adsorption sites become accessible, causing absorption rates to rise[40, 43].

6.5. Effect of time and Sonication time

Figure 7F reveals that increasing the sonication time has a positive effect on improving the percentage of sulfur removed until reaching its highest value at 40 minutes to facilitate the adsorption of sulfur molecules, and thus the contact time is reduced to reach the state of equilibrium, so the contact time and sonication time are considered complementary to each other. This trend has been confirmed by previously published data of [37, 40].

6.5. Effect of sonication time and adsorbent dose

It is clear in Figure 7E the high efficiency of the removal process when increasing the adsorbent and sonication time. Through cavitation and streaming, ultrasound is reported to enhance mixing and adsorption capacity; this leads to an increase in the mass transfer of thiophene molecules within the pores of the adsorbent. Additionally, increasing adsorption was observed due to sonic cavitation-induced changes in pore transport, pore volume, and surface area. The present results have been confirmed by the findings of [44, 45].

7. Experimental Validation of the Optimum Condition Selection

This research aims to determine the optimum variables for sulfur removal percent by ZnO/Al_2O_3 (Response) from the regression equations. The Design Experts software was used to determine the optimum condition by CCD. The input factors were "in the range," and the response (sulfur removal percent) for the adsorbent was chosen as "maximum." The desirability value obtained =1, and the optimum conditions to achieve the maximum removal percent was 69.90% for ZnO/Al_2O_3, where the optimum is: contact time = 117 min, the initial concentration=40 (mg/L), the dose of the adsorbent = 12.36 g/L, and sonication time = 39 min.

Additional experiments with the optimal settings for sulfur removal by adsorbent were carried out to show the statistical experimental design's validity. The sulfur removal experimental results at the optimal condition are 69%, close to the model's predicted values for the adsorbent.

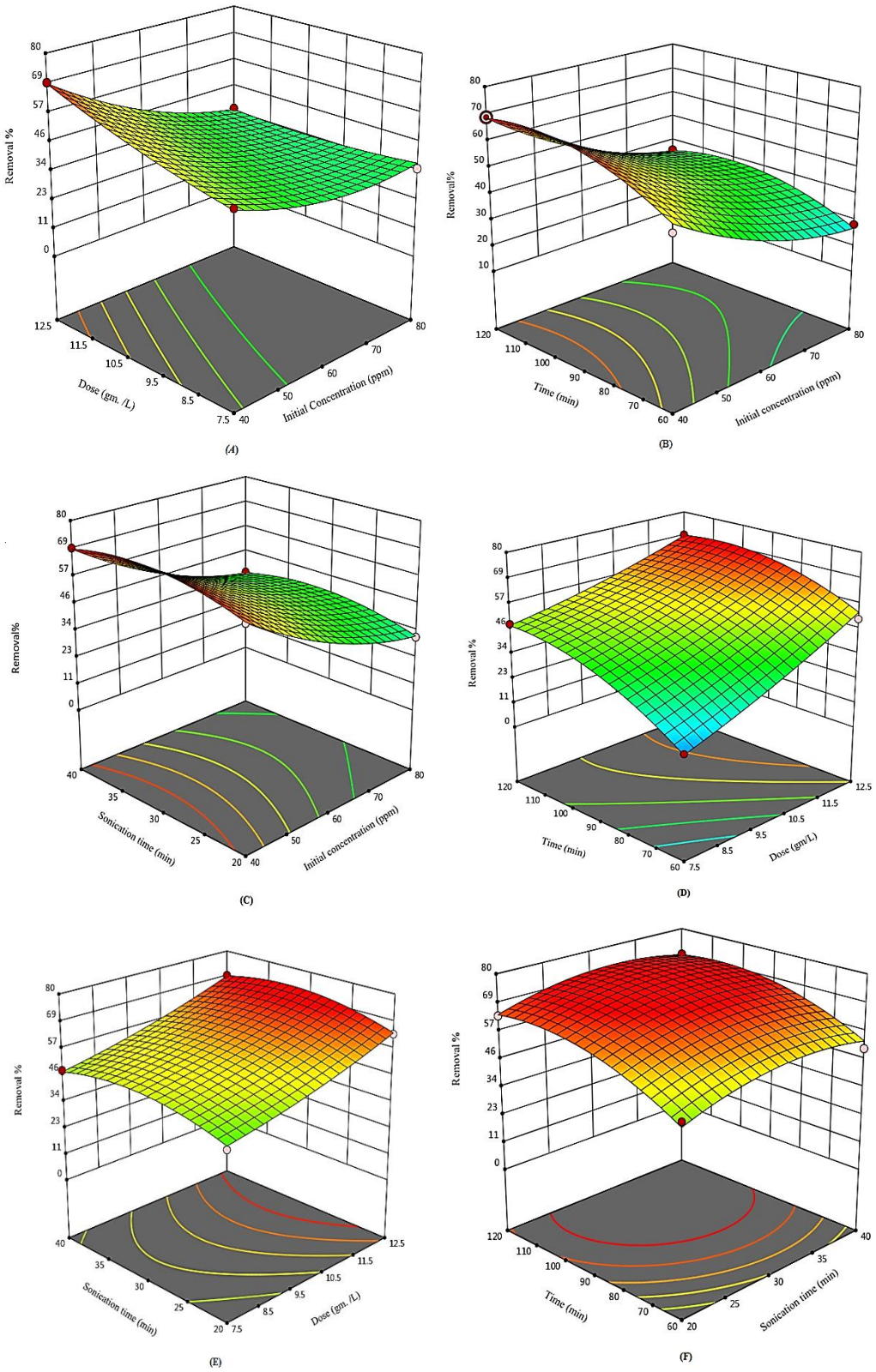

Figure 7. Variation of adsorption efficiency as a function of operating variables.

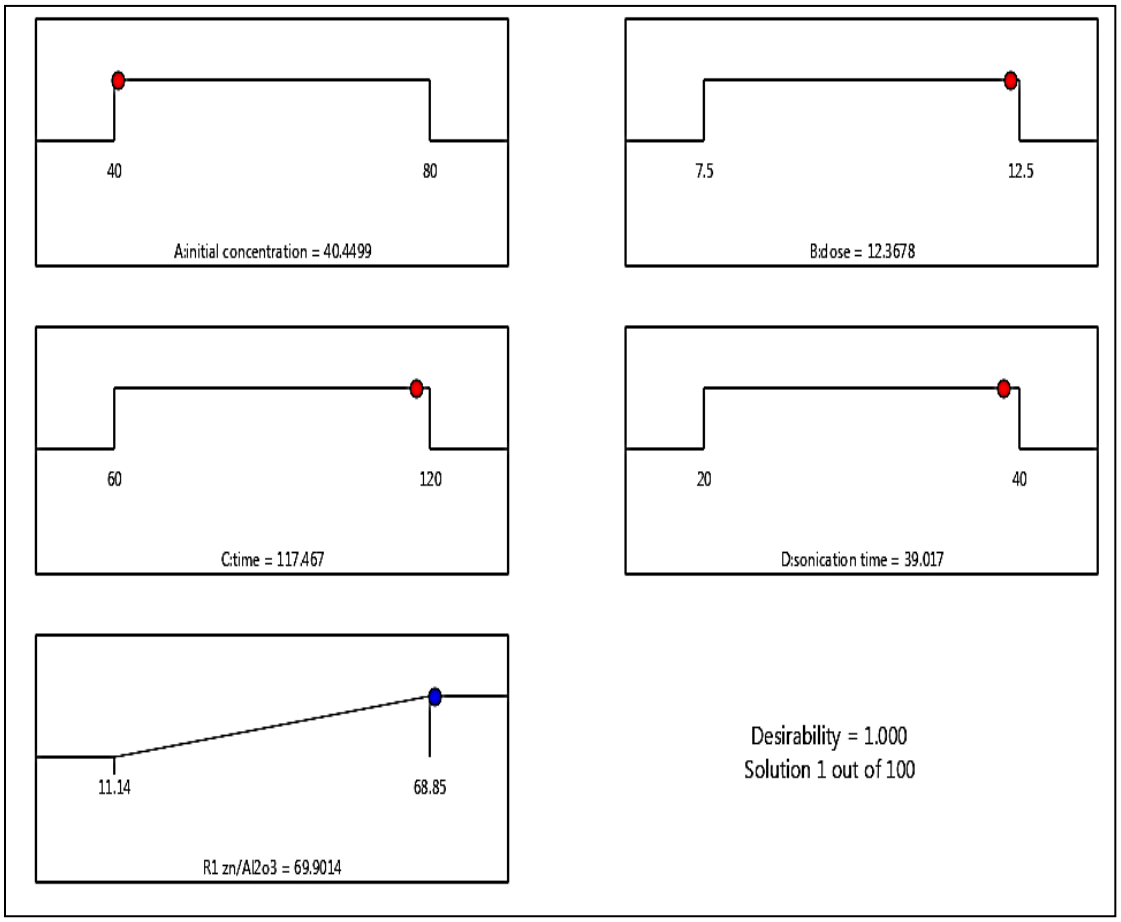

Figure 8. Optimal batch adsorption conditions for ZnO/ Al_2O_3.

8. Adsorption Isotherms

The Langmuir model isotherm for sulfur adsorption on the ZnO/Al_2O_3 is shown in Figure 9 A the associated parameters are listed in Table 7. The isotherm type is determined by the value of R_L, which ranges from linear (R_L = 1) to favourable (0 R_L 1) to unfavourable (R_L > 1) to irreversible (R_L = 0). The R_L values obtained using Eq. (4) were smaller than one, suggesting that adsorption was favored. With a correlation coefficient R^2 = 0.9985.

Freundlich isotherm model: It is also used in various adsorption techniques, shown in Figure 9B. Table 7 demonstrates that the Freundlich intensity constant is n > 1, pointing to favorable. With correlation coefficient R^2 =0.9264

Temkin isotherm model: The Temkin constants are given in Table 7, and shown in Figure 9C. The BT value refers to the process being endothermic[27]. With a correlation coefficient R^2 = 0.9372

When comparing alternative fitting models to experimental data, the coefficient of determination (R^2) is used. Due to the linearization of the Langmuir, Freundlich, and Temkin models, R^2 is 0.9985, 0.9264, and 0.9372, respectively. The Langmuir isotherm model showed the highest correlation coefficient and best fit the experimental data [46, 47].

Table 7. Parameters of isotherm models

Langmuir isotherm model		
R_L	q_m (mg/g)	R^2
0.01163	2.996704	0.9985
Freundlich isotherm model		
K_f $(mg/g)(kg/mg)^{1/n}$	n	R^2
12.38226	5.025126	0.9264
Temken isotherm model		
BT (KJ/mol)	Kt (L mg^{-1})	R^2
0.9423	17.27	0.9372

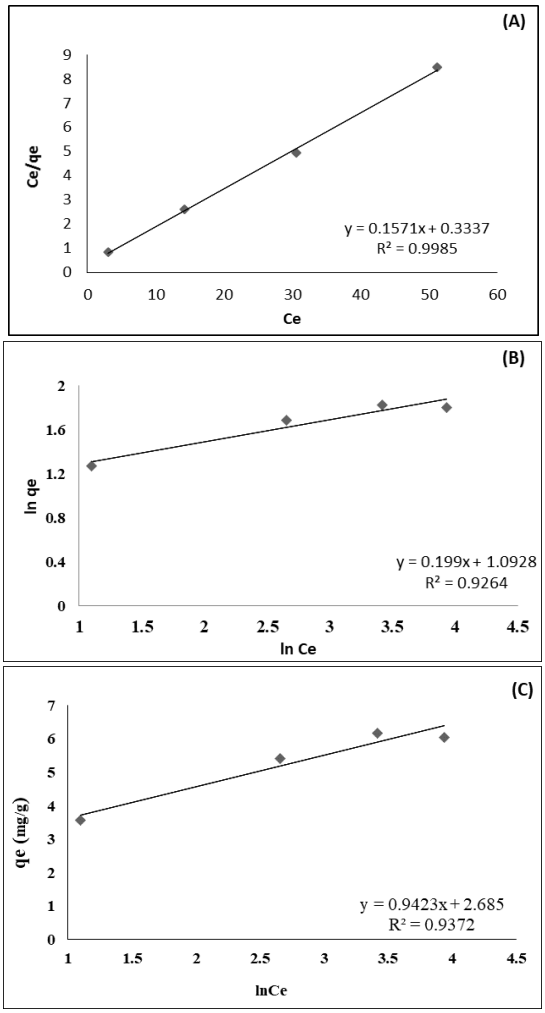

Figure 9. (A) Langmuir model, (B) Freundlich model, (C) Temkin model

9. Adsorption kinetics

Pseudo-first-order, pseudo-second-order, and intraparticle models were utilized to fit the adsorbent, and the results are shown in Table 8. Figure 10A shows the closeness of the pseudo-first-order kinetic adsorption model's predictions. As can be shown, the $R^2 = 0.9602$ suggests that the pseudo-first-order model fits well with the experimental kinetic data.

The plot of the pseudo-second-order model, which generated $R^2 = 0.8339$, is shown in Figure 10B; this value is low compared to the pseudo-first-order model. This demonstrates that the adsorption kinetics don't suit the adsorbent's experimental kinetic data.

In Figure 10 C, the plots of the intraparticle diffusion model are presented; two parts are apparent, each indicating distinct adsorption behavior. As seen in the first linear section, the adsorption capacity varies rapidly until it achieves equilibrium. This implies that the control step may be the diffusion of the boundary layer. Experimental data points were the horizontal line in the second section, indicating that equilibrium had been attained and intraparticle diffusion was occurring. The values of ki_1 and ki_2 are presented in Table 8.

Table 8. Parameters of kinetic models

Pesudo-first-order	R^2	k_1	q_e(mg/g)
	0.9602	0.0001	5.3817
Pesudo-second-order	R^2	k_2	q_e (mg/g)
	0.8339	0.0007	9.98
Intraparticle diffusion	R^2	K_i	I (mg/g)
	0.8788	0.029	1.0313

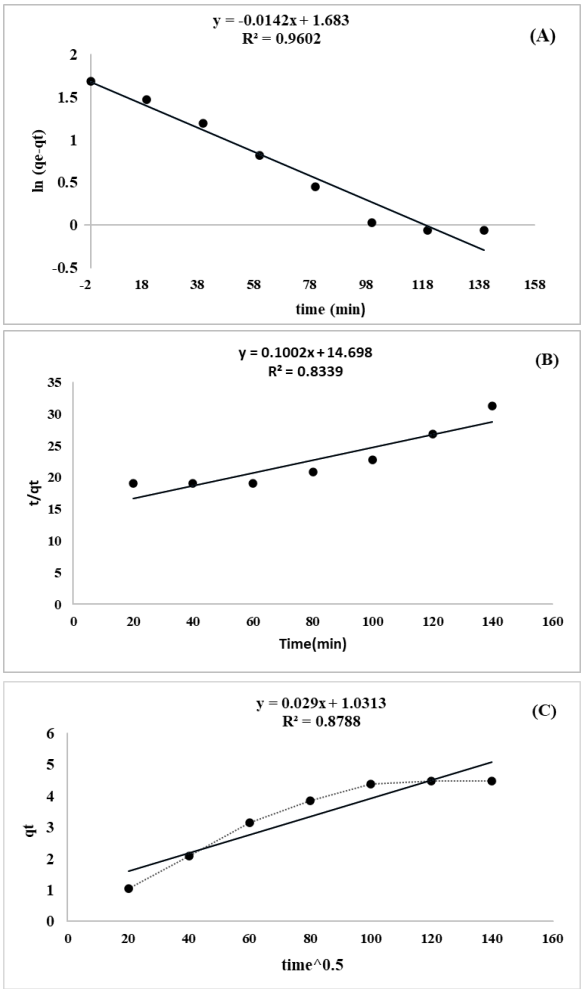

Figure 10. (A) Pseudo-first-order, (B) pseudo-second-order, and (c) intraparticle diffusion kinetic models.

10. Adsorption Thermodynamics

In Table 9, the positive values of ΔHº display that the adsorptive desulfurization process is endothermic. The higher randomization of sulfur molecules on the solid surface than in solution is confirmed by the positive value of ΔS°[48]. Since ΔS° and ΔHº both have a positive value, this means that the reaction is not spontaneous at low temperatures, so ΔGº appears with a positive value, but when the temperatures rise, it changes to negative. The reaction becomes spontaneous, according to the equation (13)[49]:

$$\Delta G^\circ = \Delta H^\circ - T\,\Delta S^\circ \qquad (13)$$

A reduction in Gibbs free energy (ΔGº) value being negative indicates the spontaneity and feasibility of the adsorption process. With the rising in temperature settings, ΔGº decreases, implying that adsorption is more favorable at higher temperatures. These results were in agreement with the research published by [50, 51].

Table 9. Thermodynamic parameters

Temp. k	ΔG°(Jmol^{-1})	ΔH°(kJmol^{-1})	ΔS°(JK^{-1}mol^{-1})
313	2452.022		
318	1223.28		
323	-361.495	78.26	242.42
328	-1048.84		

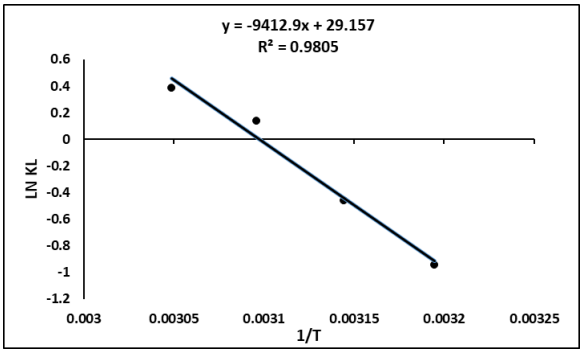

Figure 11. Thermodynamic for the desulfurization by ZnO/Al_2O_3

11. Comparison with previous work

The outcomes of the present work have been compared with previously published data to confirm the feasibility. Figure 12 plots the effect of weight percentage loading of ZnO on the adsorption capacity of sulfur for the present work and that of Yang [52].

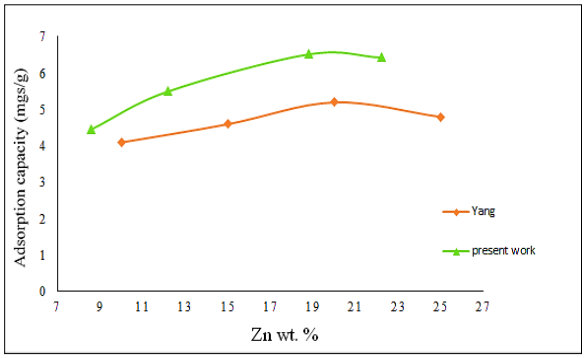

Figure (12). Variation of adsorption capacity of sulfur for the presen work and that of Yang [52]

Even though the two works using the same weight percentage loading of ZnO, the same preparation method (i.e., sol gel) of ZnO/Al_2O_3, and the same sulfur compound (i.e., thiophene), it is observed from Figure 12 that the adsorption capacity of sulfur for the present work is dominant by approximately 60 % over that attained by Yang [52]. The reason for that may be the type of Al_2O_3 which is in our work was activated alumina but in the work of Yang was γ-alumina. Srivastav et al. [10] proved experimentally that activated alumina has a good affinity for sulfur component (as DBT) adsorption.

12. Conclusion

The present study shows that the ZnO over activated alumin could be used as adsorbent for the desulfurization of liquid fuels. SEM, XRD, BET and FTIR studies were performed to understand the synthesis mechanism of ZnO/ activated alumina. Equilibrium between the thiophene in the solution and on the adsorbent surface was practically achieved in 2 h.

The optimal working parameters were 117 minutes, 40 ppm, 12.3 g adsorbent dosage, ZnO loading ratio of 18.8 wt. %, and 39 minutes of sonication duration, yielding a desulfurization efficiency of 68.8%. Langmuir isotherm best represented the equilibrium adsorption data at all temperatures. The adsorption of thiophene onto activated alumina was found to be endothermic in nature with the heat of adsorption being 78.26 kJ/mol, as well as the reduction in ΔG value with increasing temperatures signifies spontaneity and feasibility.

Acknowledgments

The authors are grateful to the Chemical Engineering Department, the University of Technology for providing space and facilitating to conducting of the present work.

Conflict of Interest

The authors declare that their present work has no conflict of interest.

References

[1]. Suryawanshi N. B., Studies in desulfurization of transportation fuels, in Engineering Sciences. 2018, AcSIR - Academy of Scientific & Innovative Research: India. p. 233.

[2]. Watanabe S., Ma X., and Song C., Adsorptive desulfurization of jet fuels over TiO2-CeO2 mixed oxides: Role of surface Ti and Ce cations. *Catalysis Today*. **371**: p. 265-275(2021)

[3]. Abid M. F., Ahmed S. M., AbuHamid W. H., and Ali S. M., Study on novel scheme for hydrodesulfurization of middle distillates using different types of catalyst. *Journal of King Saud University - Engineering Sciences*. **31**(2): p. 144-151(2019)

[4]. Kaze O. EIA expects U.S. petroleum trade to shift toward net imports during 2022. 2022 [cited 2022; Available from: https://www.eia.gov/todayinenergy/.

[5]. Muzic M., Sertic-Bionda K., Gomzi Z., Podolski S., and Telen S., Study of diesel fuel desulfurization by adsorption. *Chemical Engineering Research and Design*. **88**(4): p. 487-495(2010)

[6]. Mahmood L. H. and Abid M. F., Dmetallization of Iraqi Crude oil by Using Zeolite A. *Indian Chemical Engineer*. **62**(1): p. 92-102(2020)

[7]. Ibrahim N. K. and Aljanabi S. K., Desulfurization and Kinetic Study of Diesel Fuel by Batch Adsorption on Activated Carbon. *Engineering and Technology Journal*. **33**(8): p. 16(2015)

[8]. Yi H., Yang Z., Tang X., Zhao S., Gao F., Wang J., Huang Y., Ma Y., and Chu C., Novel synthesis of MeOx (Ni, Cu, La)@Nano-Co3O4 from combination of complexation and impregnation in ultrasonic intervention for low temperature oxidation of toluene under microwave radiation. *Ultrasonics Sonochemistry*. **40**: p. 543-551(2018)

[9]. Chong S., Zhang G., Zhang N., Liu Y., Zhu J., Huang T., and Fang S., Preparation of FeCeOx by ultrasonic impregnation method for heterogeneous Fenton degradation of diclofenac. *Ultrasonics sonochemistry*. **32**: p.231-240(2016)

[10]. Ankur S. and Vimal C. S., Adsorptive desulfurization by activated alumina. *Journal of Hazardous Materials*. **170:** p.1133–1140(2009)

[11] Dehghani M. H., Yetilmezsoy K., Salari M., Heidarinejad Z., Yousefi M., and Sillanpää M., Adsorptive removal of cobalt (II) from aqueous solutions using multi-walled carbon nanotubes and γ-alumina as novel adsorbents: Modelling and optimization based on response surface methodology and artificial neural network. *Journal of Molecular Liquids*. **299**: p.112154(2020)

[12] Yahya R. O. H., Polyoxometalate catalysis for oxidative desulfurization. The University of Liverpool (United Kingdom) (2015)

[13] Iftekhar S., Küçük M. E., Srivastava V., Repo E., and Sillanpää M., Application of zinc-aluminium layered double hydroxides for adsorptive removal of phosphate and sulfate: equilibrium, kinetic and thermodynamic. *Chemosphere*. **209:** p.470-479(2018)

[14] Baumgarten E., and Kirchhausen-Düsing U., Sorption of metal ions on alumina. *Journal of colloid and interface science* **194**(1): p.1-9 (1997)

[15] Trainor T. P., Brown Jr, G. E., and Parks G. A., Adsorption and precipitation of aqueous Zn (II) on alumina powders. *Journal of Colloid and Interface Science*. **231**(2): p.359-372(2000)

[16] Etemadi O., and Yen T. F., Surface characterization of adsorbents in ultrasound-assisted oxidative desulfurization process of fossil fuels. *Journal of colloid and interface science*. **313**(1); p.18-25(2007)

[17] Kim J. H., Ma X., Zhou A., and Song C., Ultra-deep desulfurization and denitrogenation of diesel fuel by selective adsorption over three different adsorbents: A study on adsorptive selectivity and mechanism. *Catalysis Today*. **111**(1-2): p.74-83(2006)

[18]. 2021 [cited 2022; Available from: https://prdc.oil.gov.iq/.

[19]. Conference on Aviation and Alternative Fuels, in CAAF/09-WP/05 16/10/09, . 2009, ICAO: Red Janeiro, Brazil.

[20]. AbdulRazak A. A., Shakor Z. M., and Rohani S., Optimizing Biebrich ScaR$_L$et removal from water by magnetic zeolite 13X using response surface method. *Journal of Environmental Chemical Engineering*. **6**(5): p. 6175-6183(2018)

[21]. Shakor Z. M., AbdulRazak A. A., and Shuhaib A. A., Optimization of process variables for hydrogenation of cinnamaldehyde to cinnamyl alcohol over a Pt/SiO2 catalyst using response surface methodology. *Chemical Engineering Communications*: p. 1-17(2021)

[22]. Darwish A. A. A., Rashad M., and Al-Aoh H. A., Methyl orange adsorption comparison on nanoparticles: Isotherm, kinetics, and thermodynamic studies. *Dyes and Pigments*. **160**: p. 563-571(2019)
[23]. Mohammed M. I., Abdul Razak A. A., and Hussein Al-Timimi D. A., Modified Multiwalled Carbon Nanotubes for Treatment of Some Organic Dyes in Wastewater. *Advances in Materials Science and Engineering*. **2014**: p. 201052(2014)
[24]. Maamoun I., Eljamal R., Falyouna O., Bensaida K., Sugihara Y., and Eljamal O., Insights into kinetics, isotherms and thermodynamics of phosphorus sorption onto nanoscale zero-valent iron. *Journal of Molecular Liquids*. **328**: p. 115402(2021)
[25]. Sabri A. A., Albayati T. M., and Alazawi R. A., Synthesis of ordered mesoporous SBA-15 and its adsorption of methylene blue. *Korean Journal of Chemical Engineering*. **32**(9): p. 1835-1841(2015)
[26]. Yao Y., Bing H., Feifei X., and Xiaofeng C., Equilibrium and kinetic studies of methyl orange adsorption on multiwalled carbon nanotubes. *Chemical Engineering Journal*. **170**(1): p. 82-89(2011)
[27]. Khalaf I. H., Al-Sudani F. T., AbdulRazak A. A., Aldahri T., and Rohani S., Optimization of Congo red dye adsorption from wastewater by a modified commercial zeolite catalyst using response surface modeling approach. *Water Science and Technology*. **83**(6): p. 1369-1383(2021)
[28]. Danmaliki G. I. and Saleh T. A., Effects of bimetallic Ce/Fe nanoparticles on the desulfurization of thiophenes using activated carbon. *Chemical Engineering Journal*. **307**: p. 914-927(2017)
[29]. Alardhi S. M., Alrubaye J. M., and Albayati T. M., Adsorption of Methyl Green dye onto MCM-41: equilibrium, kinetics and thermodynamic studies. *Desalination and Water Treatment*. **179**: p. 323-331(2020)
[30]. AbdulRazak A. A. and Rohani S., Sodium Dodecyl Sulfate-Modified Fe₂O₃/Molecular Sieves for Removal of Rhodamine B Dyes. *Advances in Materials Science and Engineering*. **2018**: p. 3849867(2018)
[31]. Al-dahri T., AbdulRazak A. A., and Rohani S., Preparation and characterization of Linde-type A zeolite (LTA) from coal fly ash by microwave-assisted synthesis method: its application as adsorbent for removal of anionic dyes. *International Journal of Coal Preparation and Utilization*: p. 1-14(2020)
[32]. Majid Z., AbdulRazak A. A., and Noori W. A. H., Modification of Zeolite by Magnetic Nanoparticles for Organic Dye Removal. *Arabian Journal for Science and Engineering*. **44**(6): p. 5457-5474(2019)
[33]. Bhandari V. M., Ko C. H., Park J. G., Han S.-S., Cho S.-H., and Kim J.-N., Desulfurization of diesel using ion-exchanged zeolites. *Chemical Engineering Science*. **61**(8): p. 2599-2608(2006)
[34]. Neubauer R., Husmann M., Weinlaender C., Kienzl N., Leitner E., and Hochenauer C., Acid base interaction and its influence on the adsorption kinetics and selectivity order of aromatic sulfur heterocycles adsorbing on Ag-Al2O3. *Chemical Engineering Journal*. **309**: p. 840-849(2017)
[35]. Li T.-S., Li J.-T., and Li H.-Z., Modified and convenient preparation of silica impregnated with silver nitrate and its application to the separation of steroids and triterpenes. *Journal of Chromatography A*. **715**(2): p. 372-375(1995)
[36]. Ahmedzeki N. S. and Ibrahem B. J., Reduction of Sulfur Compounds from Petroleum Fraction Using Oxidation-Adsorption Technique. *Iraqi Journal of Chemical and Petroleum Engineering* **16**(1): p. 35-48(2015)
[37]. Suryawanshi N. B., Bhandari V. M., Sorokhaibam L. G., and Ranade V. V., Investigating Adsorptive Deep Desulfurization of Fuels Using Metal-Modified Adsorbents and Process Intensification by Acoustic Cavitation. *Industrial & Engineering Chemistry Research*. **58**(18): p. 7593-7606(2019)
[38]. Rabia A. R., Ibrahim A., and Zulkepli N. Preparation and Characterization of Activated Alumina. in *E3S Web of Conferences*. 2018. EDP Sciences.
[39]. Xu C., Sun J., Zhao B., and Liu Q., On the study of KF/Zn(Al)O catalyst for biodiesel production from vegetable oil. *Applied Catalysis B: Environmental*. **99**(1): p. 111-117(2010)
[40]. Ali F. D., Adsorptive Desulfurization of Liquid Fuels Using Na-Bentonite Adsorbents. *Al-Nahrain Journal for Engineering Sciences (NJES)* **21**(2): p. 248–252(2018)
[41]. Ishaq M., Sultan S., Ahmad I., Ullah H., Yaseen M., and Amir A., Adsorptive desulfurization of model oil using untreated, acid activated and magnetite nanoparticle loaded bentonite as adsorbent. *Journal of Saudi Chemical Society*. **21**(2): p. 143-151(2017)
[42]. Jabbar S. M., Investigation on the desulfurization process inspouted bed reactors in Chemical Engineering. 2013, University of Technology: Iraq. p. 151.
[43]. Ahmad W., Ahmad I., Ishaq M., and Ihsan K., Adsorptive desulfurization of kerosene and diesel oil by Zn impregnated montmorollonite clay. *Arabian Journal of Chemistry*. **10**: p. S3263-S3269(2017)

[44]. Yao Y.-C. and Tsai J.-H., Effects of gasoline aromatic content on emissions of volatile organic compounds and aldehydes from a four-stroke motorcycle. *Environmental Technology*. **34**(17): p. 2531-2539(2013)

[45]. Bu J., Loh G., Gwie C. G., Dewiyanti S., Tasrif M., and Borgna A., Desulfurization of diesel fuels by selective adsorption on activated carbons: Competitive adsorption of polycyclic aromatic sulfur heterocycles and polycyclic aromatic hydrocarbons. *Chemical Engineering Journal*. **166**(1): p. 207-217(2011)

[46]. Yekeen N., Al-Yaseri A., Idris A. K., and Khan J. A., Comparative effect of zirconium oxide (ZrO2) and silicon dioxide (SiO2) nanoparticles on the adsorption properties of surfactant-rock system: Equilibrium and thermodynamic analysis. *Journal of Petroleum Science and Engineering*. **205**: p. 108817(2021)

[47]. Subramanyam B. and Das A., Linearised and non-linearised isotherm models optimization analysis by error functions and statistical means. *Journal of Environmental Health Science and Engineering*. **12**(1): p. 92(2014)

[48]. Olajire A. A., Abidemi J. J., Lateef A., and Benson N. U., Adsorptive desulphurization of model oil by Ag nanoparticles-modified activated carbon prepared from brewer's spent grains. *Journal of Environmental Chemical Engineering*. **5**(1): p. 147-159(2017)

[49]. Prue J., General and physical chemistry. Chapter 1. Introduction. *Annual Reports on the Progress of Chemistry, Section A: General Physical and Inorganic Chemistry*. **68**: p. 1-1(1971)

[50]. Samaniego M. L., de Luna M. D. G., Ong D. C., Wan M.-W., and Lu M.-C., Isotherm and Thermodynamic Studies on the Removal of Sulfur from Diesel Fuel by Mixing-Assisted Oxidative–Adsorptive Desulfurization Technology. *Energy & Fuels*. **33**(2): p. 1098-1105(2019)

[51]. Choi A. E. S., Roces S., Dugos N., and Wan M.-W., Adsorption of benzothiophene sulfone over clay mineral adsorbents in the frame of oxidative desulfurization. *Fuel*. **205**: p. 153-160(2017)

[52]. Yang X., Sol-gel Synthesized Nanomaterials for Environmental Applications, PhD thesis, Kansas State University (2008)